Supplemental Methods.

To calculate the ^{13}C-bicarbonate uptake by individual *L. ochracea* cells, the data were first evaluated using statistical analyses and then used for uptake calculations.

The Poisson errors in the collected data were examined using a scatterplot (Figure S3). Poisson errors did not correlate with the measured $^{13}C/^{12}C$ ratio (Pearson correlation was 0.374), with *L. ochracea* cells and filter ROIs both behaving in a similar pattern. Based on the filter data Poisson error, any ROIs exhibiting a Poisson error greater than 0.006904808 were eliminated from further analysis (similarly performed in 1). With the remaining filter ROIs, the mean $^{13}C/^{12}C$ ratio was calculated per run (Filter Mean). For each run, the adjusted $^{13}C/^{12}C$ ratio was then calculated by subtracting the mean of the accumulated data $^{13}C/^{12}C$ ratio for each *L. ochracea* cell $^{13}C/^{12}C$ ratio or filter ROI $^{13}C/^{12}C$ ratio minus the mean $^{13}C/^{12}C$ ratio for the filter. (Adjusted Ratio = Mean ratio - Filter Mean).

To understand the distribution of adjusted $^{13}C/^{12}C$ ratios, the distribution of the adjusted ratios was visualized using box plots with a violin plot overlay (Figure S4). Filter ROIs had a variation in $^{13}C/^{12}C$ ratios that was consistent with natural instrumental background variation and slightly different tuning of the nanoSIMS instrument during the different measurement sessions The *L. ochracea* cells exhibited an enrichment beyond the filter distribution. *L. ochracea* cells that were incubated, not incubated with ^{13}C-bicarbonate, and their respective filters were compared separately. The adjusted $^{13}C/^{12}C$ ratio for incubated *L. ochracea* cells was greater, but there was insufficient unincubated data to make statistical comparisons. The negative adjusted $^{13}C/^{12}C$ ratios of the unincubated *L. ochracea* cells were not unexpected. The Lakeside Drive (LD) waters

come from an upstream wetland bog and the carbon source for *L. ochracea* could be either from decomposed vegetation or from CO_2-derived microbial decay of decomposed vegetation. Both of these carbon sources are generally depleted in ^{13}C-carbon relative to carbon assimilated from atmospheric CO_2-fixation (2).

To calculate the total cell inorganic carbon assimilation and assimilation rates for the *L. ochracea* cells, the biovolume and total carbon for each cell was calculated and then the ^{13}C and the ^{12}C carbon assimilated was calculated. The total C contained in a cell was calculated assuming a cell contains 2160 attomol C $cell^{-1}$ (3) and a cell is 2.094 μm^3 in size. Individual *L. ochracea* cell biovolumes were calculated using the size and LW ratio for each ROI and the formula for the volume of a cylinder (biovolume = π x (0.5 x size)^2 x length width ratio (0.5 x size)). To determine carbon total assimilation the adjusted ratio was multiplied by the total C contained in a cell and divided by the experimentally added ^{13}C-bicarbonate / (^{12}C-bicarbonate + ^{13}C-bicarbonate) ratio; 1:10. To present the data as total assimilation of carbon relative to unincubated cells, the mean calculated assimilation value for the unincubated cells (13.07 attomol C assimilated $cell^{-1}$) was added to all cells (Figure 4). Finally, the total the attomol C $cell^{-1}$ hr^{-1} were calculated. The R (4-6) software package was used for all data processing, plots and calculations of means, medians, minimums, maximums, and standard deviations.

References

1. **Kopf SH, McGlynn SE, Green-Saxena A, Guan Y, Newman DK, Orphan VJ.** 2015. Heavy water and (15) N labelling with NanoSIMS analysis reveals growth rate-dependent metabolic heterogeneity in chemostats. Environ Microbiol **17**:2542–2556.

2. **Clark ID, Fritz P.** 1997. Environmental isotopes in hydrogeology. CRC Press.

3. **Troussellier M, Bouvy M, Courties C.** 1997. Variation of carbon content among bacterial species under starvation condition. Aquat Microb Ecol **13**:113–119.

4. **Wickham H.** 2016. ggplot2: Elegant graphics for data analysis. Springer-Verlang, New York.

5. **Wickham H, Francois R.** 2016. dplyr: a grammar of data manipulation. R package version 0.5.0. https://CRAN.R-project.org/package=dplyr.

6. **R Core Team.** 2016. R: A language and environment for statistical computing. R Foundation for Statistical Computing, Vienna, Austria. URL https://www.R-project.org/

Figure S1

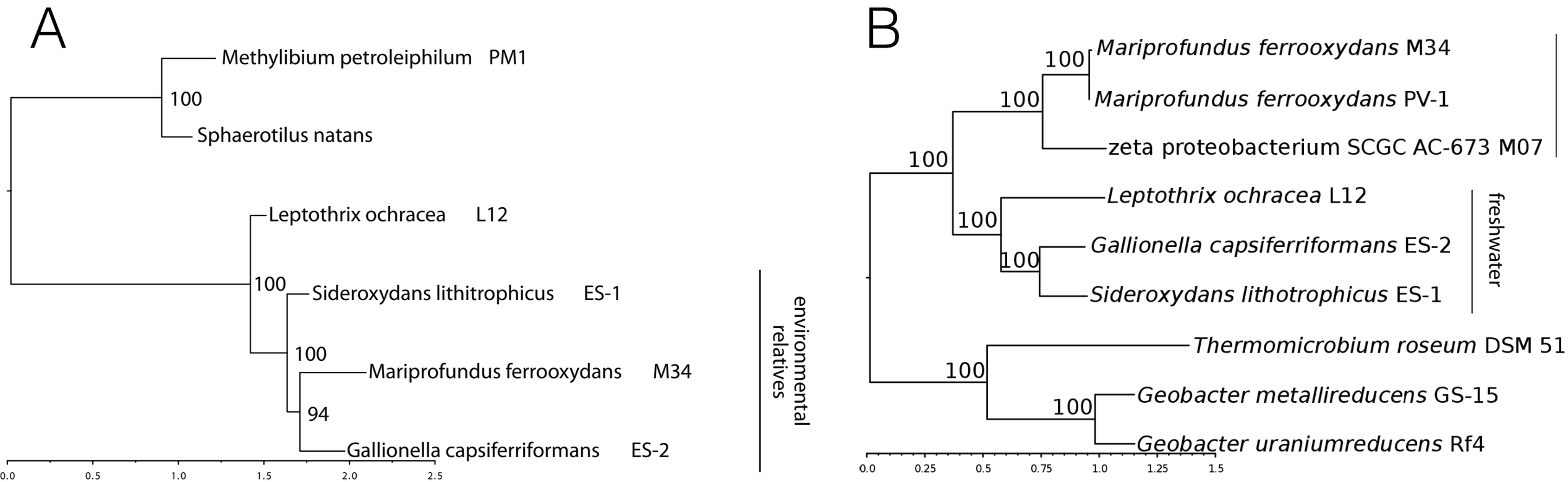

Figure S1. Phylogenetic relationship of proteins proposed to be involved in iron-oxidation in FeOB. The maximum likelihood tree was generated for the cytochrome bd oxidase protein sequences (A) and AC complex II molybdopterin oxidoreductase (B). Protein sequences were aligned in Clustal omega and tree was generated using the rapid bootstrap method with 100 bootstraps in RAxML. *L. cholodnii* SP-6 did not have either genes and thus was not be included in the analysis.

Figure S2

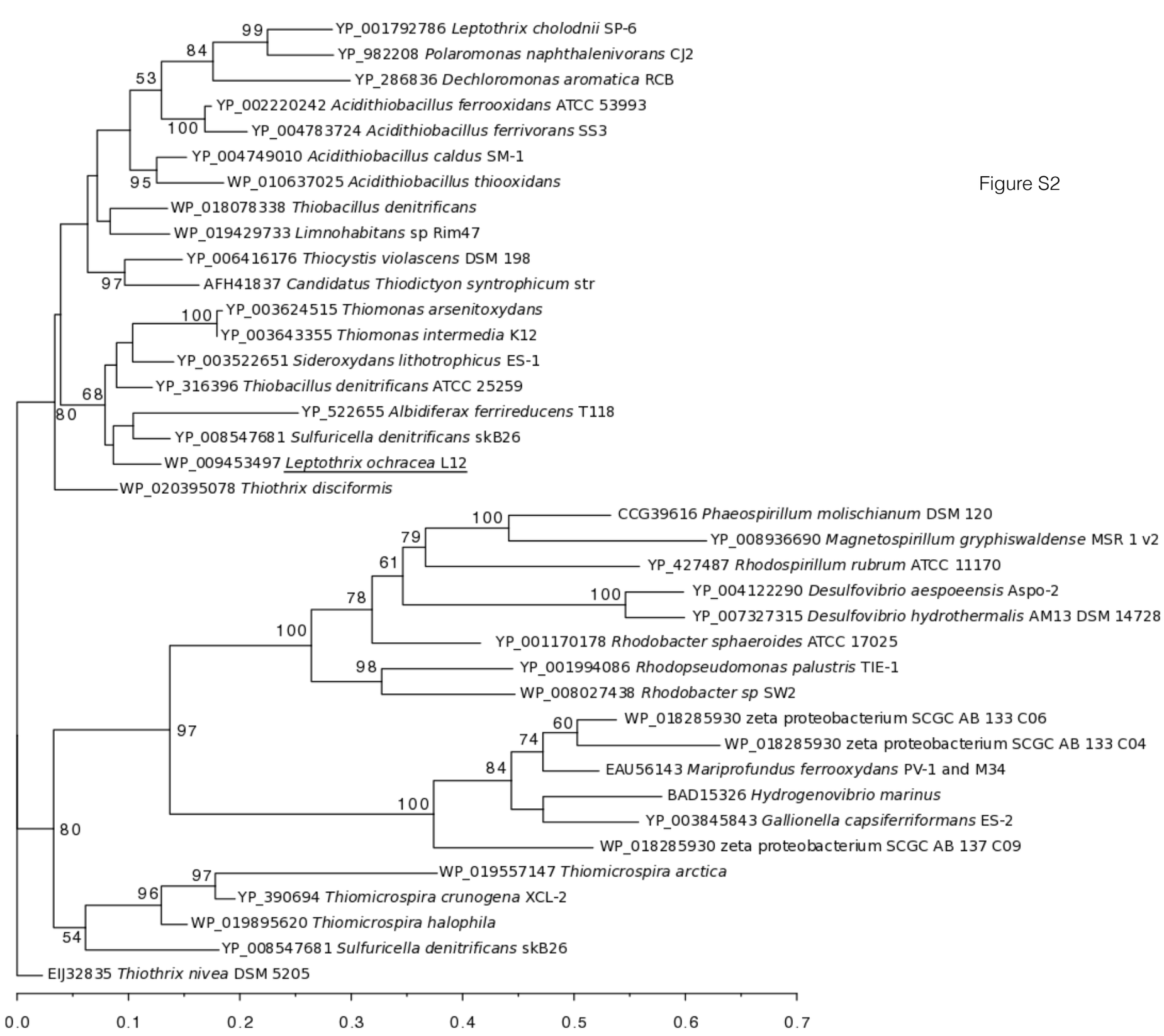

Figure S2. The phylogenetic relationship of Form II RubisCO protein sequences. Some Sulfur oxidizing bacteria, Sequences did not group together based on common habitat (A), the position of the RubisCO sequence from *L. ochracea* is bolded and the positions of RubisCO sequences from other neutrophilic iron-oxidizing bacteria are underlined. Protein sequences were aligned in Clustal Omega and the maximum likelihood tree was generated with 1000 bootstraps in RAxML. Only those bootstraps above 50 are displayed on the tree.

Figure S3

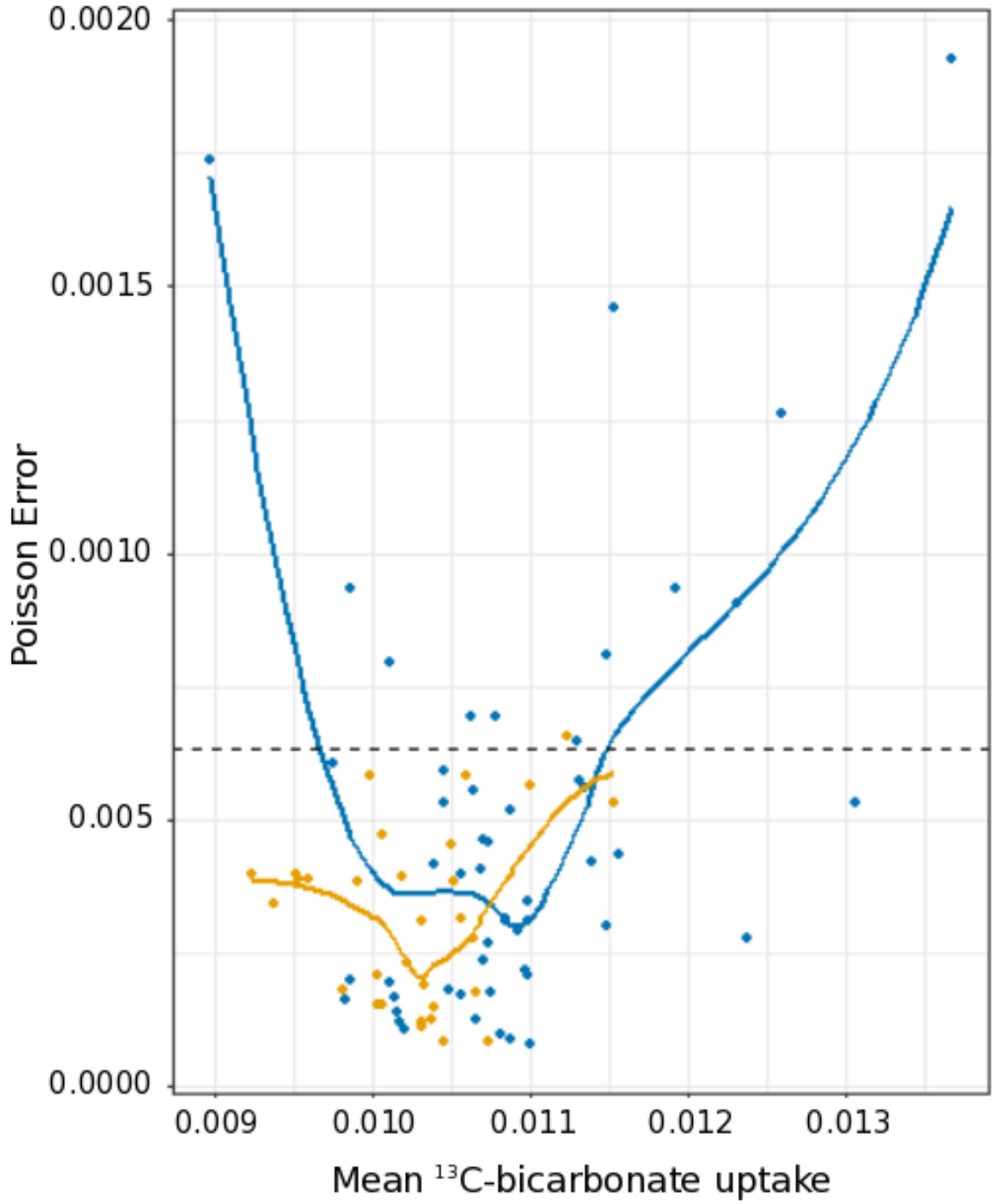

Figure S3. Scatter plot of the mean $^{13}C/^{12}C$ ratios vs. Possion error for all the *L. ochracea* (blue) and filter ROI (yellow) analyzed. Dashed line represents twice the mean Poisson error measured for filter ROI. The ROI greater than the dashed line were excluded from further analysis.

Figure S4

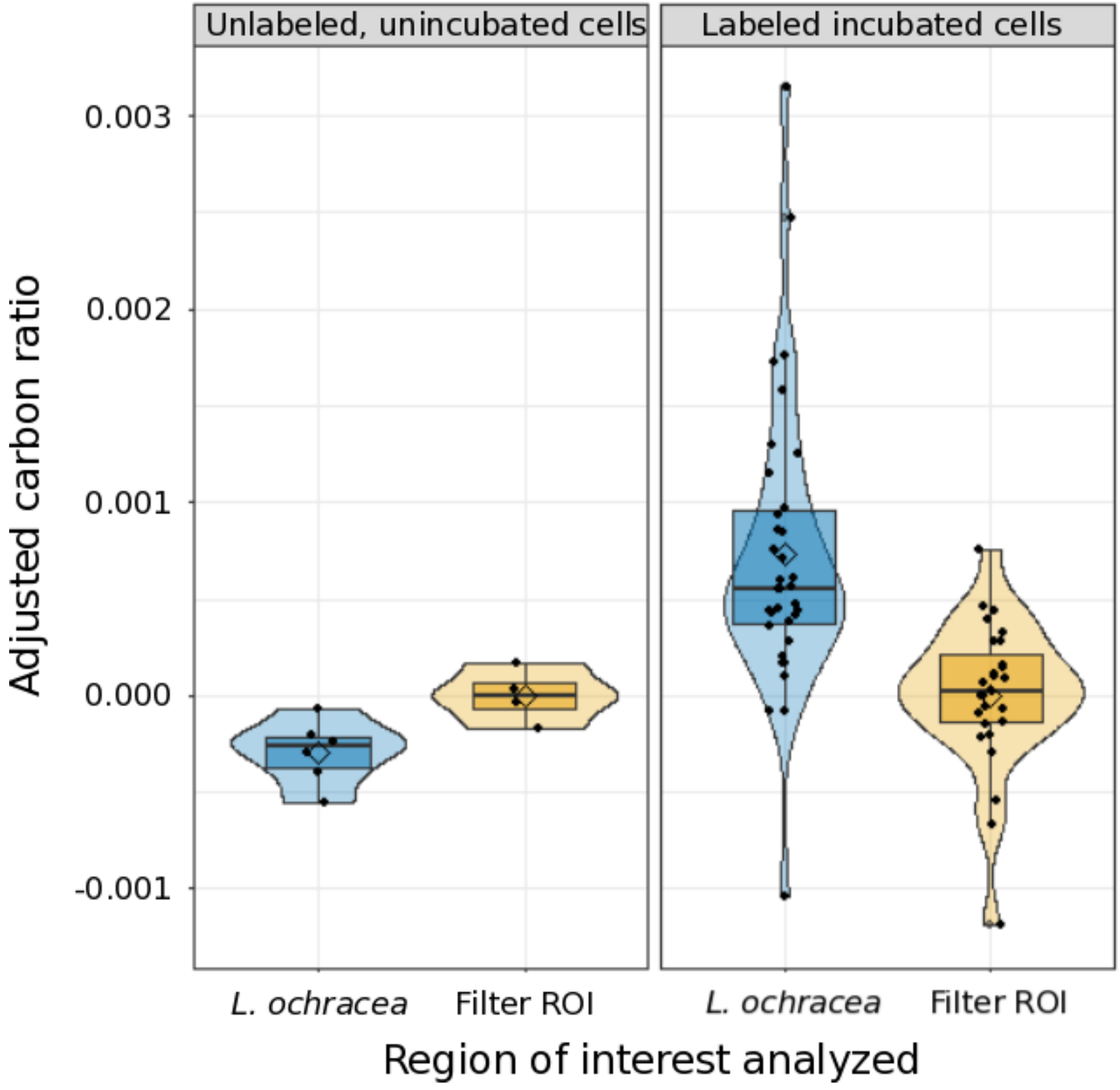

Figure S4. Violin plot with box plot overlay of the adjusted carbon ratio from filters containing uninncubated innoculum (A) and incubated innoculum (B) for *L. ochracea* cells (blue) or filter ROIs (yellow).